

# Passive Perching with Energy Storage for Winged Aerial Robots

William Stewart,\* Luca Guarino, Yegor Piskarev, and Dario Floreano

Perching in unmanned aerial vehicles (UAVs) offers the possibility of extending the range of aerial robots beyond the limits of their batteries. It has been a topic of intense study for multirotor UAVs. Perching in winged UAVs is harder because a kinetic energy balance has to be struck. Reducing too much energy results in the vehicle stalling and falling. Too much kinetic energy at touchdown could damage the vehicle. Most studies used dangerous pitch-up maneuvers to manage this balance. This work presents a system that eliminates the pitch-up maneuver by mechanically capturing and storing kinetic energy at impact. It is validated using a passive mechanical system consisting of a storage mechanism for energy recuperation and a claw for perching on a horizontal rod. The energy stored in the mechanism is then used to unperch. The mathematical model for the recuperation strategy is presented and perching success at various approach attitudes are characterized. The proof-of-concept claw recaptures 5% of the kinetic energy during perching. Experiments indicate that the device can successfully perch at a wide range of yaw angles, but requires more precision in roll. We show that our perching mechanism enables the fastest UAV perching to date ( $7.4 \text{ m s}^{-1}$ ).

speed of the aircraft to very close to stall speed. At these low speeds, the effectiveness of the control surfaces is reduced, limiting the vehicles ability to adjust its trajectory near the perching structure. Furthermore, only two works to date have directly addressed unperching and taking flight again.<sup>[15,16]</sup>

We simultaneously address both the complicated perching maneuver and unperching by adding a claw that can absorb and store kinetic energy at the moment of perching and later use that energy to reopen the claw, allowing the vehicle to unperch (Figure 1). By absorbing a portion of the kinetic energy at impact, we are not required to bleed off energy in the way that most current solutions have to. Thus, this mechanism will allow for perching at higher speeds than has been previously possible. Our solution utilizes springs to absorb the kinetic energy which


also has the effect of increasing the time of impact. This reduces the maximum impact force by spreading it out over a longer time period. As a result, our perching maneuver is more straightforward and consists of flying right into the structure without any transitional maneuvers. Because this principle passively stores kinetic energy, it has the added advantage of not requiring additional energy expenditure during perching. The claw presented here is designed for perching on large-scale linear infrastructure such as cranes, bridges, and other tall trusses. Our concept addresses the problem of complicated perching maneuvers; therefore, we do not address the challenges associated with the precision flight required for all perching solutions on linear infrastructure.

In this article we introduce and analyze the concept of recapturing lost energy of winged UAVs when perching, we characterize the performance of the novel perching mechanism in terms of impact speed, yaw angle, and holding strength, and we validate the mechanism at both low and high speeds.

## 1. Introduction

As more untethered robots take to the skies over the coming decades, they will face difficult energy storage challenges which will limit their range and endurance. One promising way to address this is to perch on structures for a short time to recharge batteries, conduct surveillance, or interact with the environment. Many interesting perching mechanisms have been proposed for multirotor and flapping wing vehicles,<sup>[1–11]</sup> but fewer have been studied for winged unmanned aerial vehicles (UAVs). Most of the perching techniques that do exist for fixed-wings require complicated maneuvers that are designed to bleed off as much kinetic energy as possible prior to contact.<sup>[12–14]</sup> To reduce kinetic energy as much as possible, the maneuvers reduce the forward

W. Stewart, L. Guarino, Y. Piskarev, D. Floreano  
School of Engineering  
École Polytechnique Fédérale de Lausanne  
Lausanne 1015, Switzerland  
E-mail: william.stewart@epfl.ch

 The ORCID identification number(s) for the author(s) of this article can be found under <https://doi.org/10.1002/aisy.202100150>.

© 2021 The Authors. Advanced Intelligent Systems published by Wiley-VCH GmbH. This is an open access article under the terms of the Creative Commons Attribution License, which permits use, distribution and reproduction in any medium, provided the original work is properly cited.

DOI: 10.1002/aisy.202100150

## 2. Related Work

Studies on perching in fixed-wing UAVs have predominantly focused on reducing kinetic energy at landing through the use of pitch-up maneuvers. These maneuvers consist of rapidly increasing the angle of attack of the UAV which simultaneously increases both lift and drag. The limitation of this strategy is that below a certain speed and above a certain angle of attack, the



**Figure 1.** Photograph of aircraft with perching claw on front.

wings will stall and would not produce enough lift, causing the vehicle to fall.<sup>[17]</sup> In addition to this, the stalled wings reduce the control power of the aircraft, leading to potentially dangerous flight conditions. A very precise control system is therefore needed to reduce speed as much as possible without stalling. To achieve such a precise controller, Cory and Tedrake created an optimized controller specific to their aircraft by using actual flight data recorded in an indoor motion capture arena.<sup>[12]</sup> The authors did not discuss a final perch speed, but stated that they needed to be as close to zero velocity as possible when they successfully perched. Desbiens et al. demonstrated a precise controller with an algorithm to analyze multiple flight controllers and ensure they could perform the touchdown maneuver.<sup>[13]</sup> The authors reported successful speeds in velocity components rather than magnitude, but found very few trajectories that were successful above  $2 \text{ m s}^{-1}$  in either component. Finally, Waldock et al. used reinforcement learning to train a controller<sup>[14]</sup> to perch precisely. They were able to show success at an average flight speed of  $3.25 \text{ m s}^{-1}$ . These three works were quite successful in dramatically reducing the vehicle speed at impact using precise maneuvers.

In previous work, we considered a different approach that avoided the need for a precise maneuver altogether.<sup>[18]</sup> We developed a spring-driven passive perching mechanism that upon impact with a wall would drive needles into the wall, which would hold up the aircraft. Although there was no need for precise maneuvers, the mechanism only worked for speeds up to  $4 \text{ m s}^{-1}$ , did not store energy for unperching, and the mechanism had to be reset by hand; furthermore, due to the shallow depth of the needles puncture, the resulting holding force was suitable only for UAVs with a weight of only a few tens of grams. A similar approach was used by Anderson et al. when developing the sticky-pad plane.<sup>[16]</sup> This UAV was equipped with a puck coated in adhesive on its nose. When impacting a flat vertical surface, the puck would stick to it, and the vehicle would hang from the puck with a cable. A blade attached to the UAV's elevator was used to cut the cable and release the aircraft. The sticky-pad plane had a few drawbacks, the first is in the use of adhesives, which often require clean surfaces, and can be susceptible to creep. As with our needle approach, the sticky-pad plane was also weight limited, and had no energy storage. Finally, a similar approach to

perching was used on a multicopter.<sup>[4]</sup> In this work, a multicopter slowly approaches a wall, where on contact, a passive aid triggers a perching maneuver that reorients the vehicle to perch on a wall. Although this work implemented a simple approach maneuver, it was done at a very small scale (38 g) and slow speed ( $0.8 \text{ m s}^{-1}$ ).

Two private companies, Insitu and Zipline, independently developed cable-based UAV recovery systems. In both systems, the UAV contacts and hooks itself onto a cable as it flies by. In the Insitu system, a vertically hanging cable contacts the wing and slides along the wing leading edge to the wingtip where the cable gets hooked, stopping the UAV.<sup>[19]</sup> The Zipline system instead relies on a horizontal cable that gets hooked on the tail of the aircraft.<sup>[20]</sup> Unlike the completely passive Insitu system, the Zipline cable is held by actively controlled robot arms that catch the aircraft. All these solutions reduce aircraft control complexity by simply commanding the aircraft to fly into the structure. However, none of these systems capture any of the kinetic energy from flight, and the only one which could unperch cannot perch on bars and rods.

### 3. Operating Principle

We study the concept of passive perching with a three-fingered claw, each composed of two phalanges (**Figure 2**). At the joints between the phalanges are rotational springs that press the fingers closed. These rotational springs passively grip the structure being perched on. Meanwhile, a second set of springs, this time linear, are stretched during the impact, thereby storing some of the kinetic energy from impact.

The claw fingers are connected by pins to a palm, which in turn is connected to a sled. The sled can slide forward and backward in a channel that runs along the fuselage from the nose to just before the leading edge of the wing. The sled is connected through four linear springs to the fuselage of the aircraft such that when the sled is all the way forward, the linear springs are in the unstretched position. Cables connect each finger to the fuselage of the aircraft. When the sled is all the way forward, these cables are pulled taut against the rotational springs, holding the fingers open (**Figure 2b**). As the sled slides back, the cables loosen and the rotational springs can close the fingers. When the sled is all the way back, the linear springs are fully stretched and the rotational springs are unstretched. Thus, by shifting the sled's position in the aircraft, spring potential energy is transferred between the rotational springs and the linear springs. A small latch at the back of the device is triggered by the sled when it is fully back and holds the linear springs in the stretched position.

The claw has a mass of 170 g and measures  $7 \times 7 \times 24 \text{ cm}$  when closed and reaches 31 cm when open. For our proof-of-concept, we mounted the claw to the nose of an off-the-shelf Easystar II UAV. This UAV is built out of foam and is pusher configured, meaning that the propeller is in the back of the aircraft, away from where the claw is mounted. The Easystar II has a wingspan of 1.37 m and length of 0.86 m and with the claw it weighs 0.85 kg.

When initially launched, the UAV claw is closed and the internal linear springs are stretched (**Figure 3a**). When approaching a perching point, the linear springs are released by a small servo

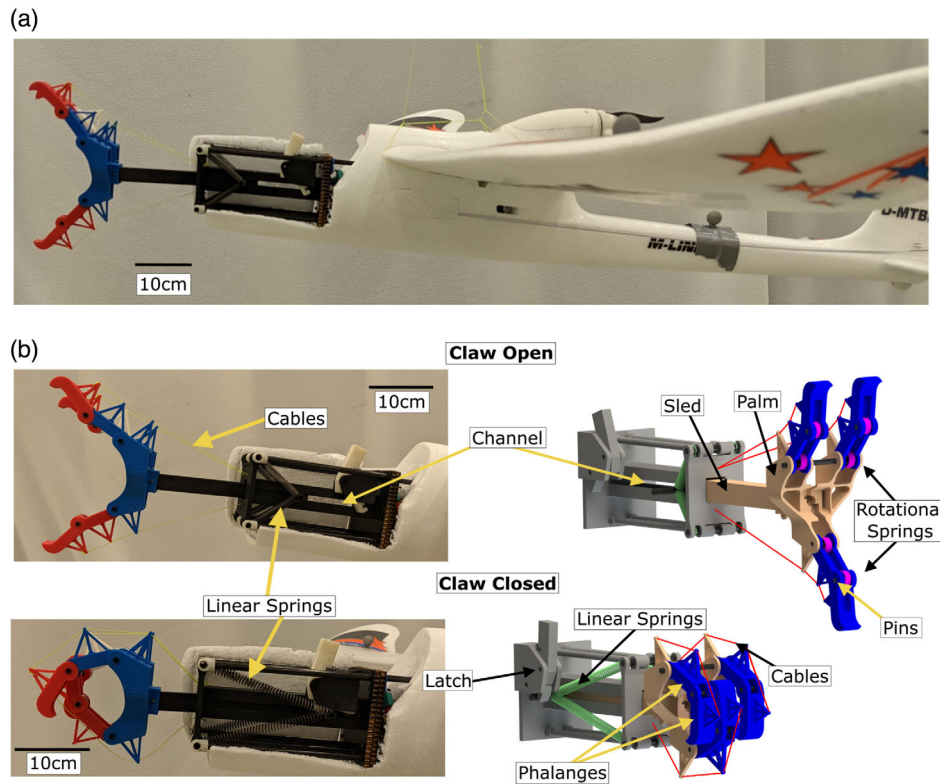


**Figure 2.** a) Photograph of the claw on the UAV. b) Left: Photos of the claw open and closed. Right: CAD of the claw open and closed. Just prior to impact, the claw is open. At impact, the palm and sled (both brown) are pushed backward along the channel, stretching the linear springs (green). This simultaneously makes the cables (red) slack, allowing the rotational springs (purple) to close the phalanges (blue) around the structure. At the back of the channel the latch (grey) engages, holding the linear springs in their stretched position and the claw closed.

where they force the sled forward and open the claw fingers, thereby transferring energy from the linear springs to the rotational springs (Figure 3b). On impact with a horizontal rod or bar structure (Figure 3c), the kinetic energy of the UAV pushes the sled backward and energy is transferred into storage in the linear springs. Simultaneously, a portion of the energy (based on the diameter of the structure being perched on) is transferred out of the rotational springs as the fingers wrap around the structure (Figure 3c). The vehicle then hangs from the structure (Figure 3d). When it comes time to take off again, the latch is released by a small servo, and the linear springs transfer their stored energy to push against the rotational springs in the fingers and open the claw (Figure 3e). This causes the aircraft to fall backward toward the ground. Winged UAVs that are stable while flying forward are quite unstable when flying backward, so the vehicle will naturally tend to turn itself around (Figure 3f).

To track the transmission of energy between the components of the system, we need a model for each component. The first component is the kinetic energy of the aircraft during flight. We do not try to account for propulsion system efficiency because what is important when perching is the amount of kinetic energy the aircraft has, not where the kinetic energy came from. The equation for kinetic energy KE is given by

$$KE = \frac{1}{2}mv^2 \quad (1)$$

where  $m$  is the mass and  $v$  is the velocity of the aircraft. Our vehicle has a mass of  $m = 0.85$  kg, and a stall speed of  $7 \text{ m s}^{-1}$ , giving a minimum KE of 21 J when perching.

The next component of the system is the fingers where energy is stored as potential energy in the rotational springs. The equation for potential energy in the rotational springs  $PE_R$  is

$$PE_R = 3 \frac{1}{2} k_R (\theta_1^2 + \theta_2^2) \quad (2)$$

where  $k_R$  is the spring stiffness in  $\text{N m rad}^{-1}$ , and  $\theta_1$  and  $\theta_2$  are the rotational displacements of the two springs in each finger relative to a rest value of  $90^\circ$  (Figure 4). Each rotational spring has the same stiffness and the factor of 3 results from the three fingers of the claw. When the claw is fully open just before perching,  $\theta_1$  has a value of  $78^\circ$  and  $\theta_2$  has a value of  $94^\circ$ . With a  $k_R$  of  $0.1263 \text{ N m rad}^{-1}$ , the potential energy in the fingers when open is 0.86 J. When perched, the rotational displacement is a function of the diameter of the structure that the vehicle is perched on. The larger the structure's diameter is, the larger the  $\theta$  values will be, and therefore the larger the amount of energy stored in the claw. Details of this function can be found in the Note S1, Supporting Information.

The potential energy stored in the linear springs  $PE_L$  can likewise be written

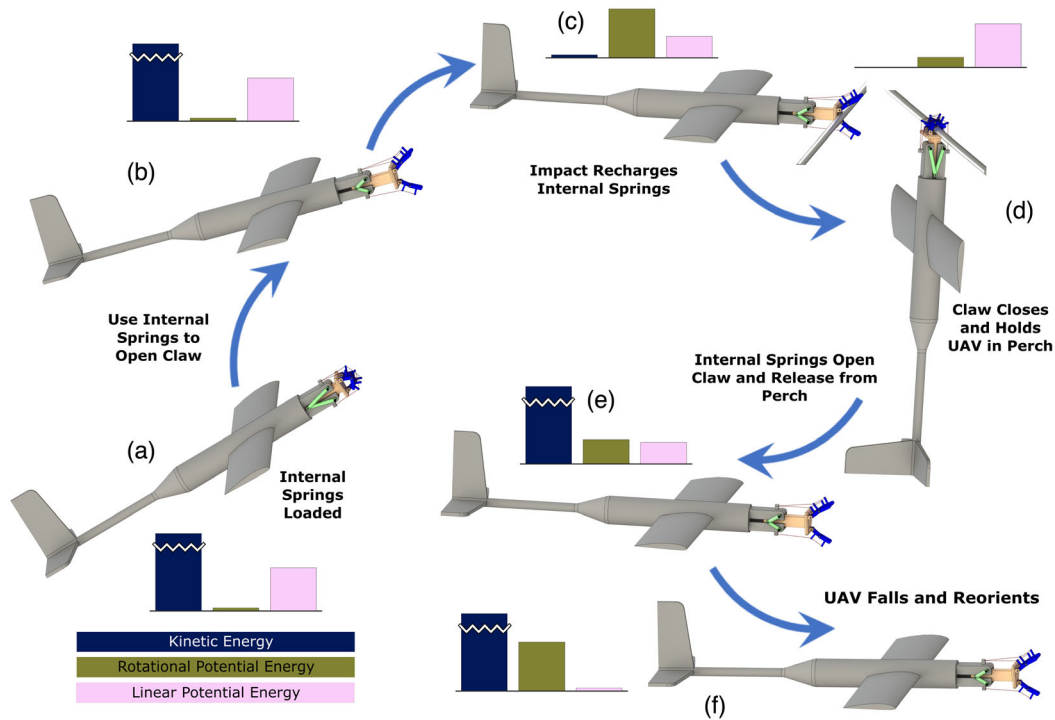


**Figure 3.** Diagram showing the stages of a potential mission for the perching mechanism developed here. a) The aircraft takes-off and cruises to the perching location. b) The aircraft releases stored energy in the linear springs to open the claw. Upon perching, c) kinetic energy is converted to spring potential energy and stored in the linear springs. While perched, d) the rotational springs hold the claw closed around the structure being perched on. When unperching, e) the energy stored in the linear springs is used to open the claw and release the aircraft. f) The UAV falls backward and passively reorients itself to fly off. Stages depicted here correspond to the stages in Table 1.

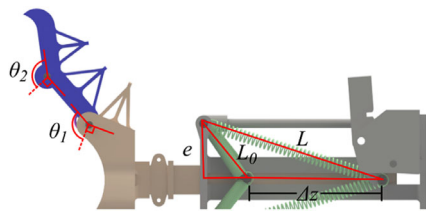


**Figure 4.** Graphic illustration of geometric values from Equation (2) and (3).  $L_0$  and  $L$  are the lengths of the linear springs unstretched and stretch, respectively.  $\theta_1$  and  $\theta_2$  are the two rotational displacements of the rotational springs. They are measured relative to the rest position, indicated with the dashed red line.

$$PE_L = 4 \frac{1}{2} k_L (L - L_0) \quad (3)$$

where  $k_L$  is the spring stiffness in  $N\ m^{-1}$  and the factor of 4 results from the four linear springs used in parallel;  $(L - L_0)$  is the linear displacement of the springs (Figure 4). Because of the latch system, the linear springs have only two stable positions: one is when they are fully stretched and being held by the latch, and the second is when they are at equilibrium with the rotational springs and the claw is open. For our claw  $k_L$  is  $208\ N\ m^{-1}$ ,  $L$  is  $107\ mm$ , and  $L_0$  is  $44\ mm$ . Thus, when the linear springs are held open the stored energy is  $1.65\ J$ .

The linear and rotational springs pull against each other; therefore, when the claw is open and not held by the latch, there is an equilibrium point where the linear springs and the rotational springs both have some small amount of stored energy. How wide open the claw is held depends on the relative stiffnesses of the two sets of springs ( $k_R$  and  $k_L$ ). For instance, a high  $k_L$  would hold the claw open wider, potentially making it easier to hit the perching structure. Softer linear springs on the other hand would hold the claw more narrowly open, while reducing the kinetic energy required at impact to stretch them. At equilibrium, our spring length  $L$  is  $77\ mm$ ; therefore, the energy stored in the linear springs is  $0.45\ J$ .

With these three models, it is possible to calculate the energy stored in each component throughout the mission (Table 1). The UAV prepares to perch by opening the claw transferring potential energy stored in the linear springs to the rotational springs in the fingers (mission stage (a) to (b) in Table 1 and Figure 3). At perching, some kinetic energy is transferred into the linear springs and some rotational energy is released from the fingers depending on the diameter of the structure being perched on (mission stage (b) to (c) in Table 1 and Figure 3). When unperching, the energy from the linear springs is used to open the claw, releasing the vehicle from the perch (mission stage (c) to (d) in Table 1 and Figure 3). At this point, the vehicle regains kinetic energy from its propulsion system (mission stage (d) to (e) in Table 1 and Figure 3). The values in Table 1 do not include the small amount of energy required to reopen the claw with a servomotor.

**Table 1.** Energy levels throughout the mission.

Mission Stage	Kinetic	Linear	Rotational	Total
(a)	21J	1.65J	0J	22.65J
(b)	21J	0.45J	0.85J	22.31J
(c)	0J	1.65J	f(diameter)	f(diameter)
(d)	0J	1.65J	f(diameter)	f(diameter)
(e)	21J	0.45J	0.86J	22.31J
(f)	21J	0.45J	0.86J	22.31J

For the claw developed in this project, we capture 1.65 J of energy from the impact, or about 5% of the kinetic energy. Meanwhile, 0.34 J is used when opening the claw before perching (total energy in the system, Table 1). Up to a further 0.34 J is used when opening the claw to unperch. This sums to a maximum of 0.68 J, or 40% of the energy that is captured at perching.

The minimum required potential energy for the rotational springs is based on the weight of the aircraft. These springs have to be able to hold onto the bar or rod from which it hangs after perching. The potential energy of the rotational springs then, in turn, defines the minimum required energy for the linear springs. This is because the linear springs must be able to reopen the claw to release the perch and to do that they must overcome the energy in the rotational springs. These requirements on the rotational energy and linear energy can be achieved either through adjustments in geometry or through spring stiffness.

#### 4. Characterizing the Effectiveness of the Claw

In order to ensure that the UAV will be able to perch at its slowest flying speed (stall speed), it is crucial to know the minimal impact speed required for triggering the perching mechanism. The experiments consisted of hanging the aircraft at the end of a pendulum consisting of a 3.26 m cable connected to the ceiling of a motion capture hall (Figure 5). The airplane was pulled back and up, and then released by hand allowing it to freely swing

downward. At the lowest point on the pendulum, when the air-plane is level there was a rigidly fixed horizontal pole with a diameter of 5.5 cm. The claw impacted the pole and closed, storing some of the kinetic energy as spring potential energy. Because there is a limited maximum achievable speed by changing the arm length of the pendulum, the weight of the aircraft was increased instead. Small weights were added to the aircraft increasing its weight to 1.15 kg. This increases the speed at impact to ensure that the setup will be capable of reaching the minimum speed required to trigger the closing of the claw. The experiment was conducted multiple times at a variety of release heights, each time recording whether the perching mechanism was triggered. Throughout the experiment, aircraft position data were captured by an Optitrack motion capture system and differentiated with time to measure the velocity, and therefore kinetic energy, at impact. The results indicate that a minimal speed of  $3.35 \text{ m s}^{-1}$  (corresponding to an impact energy of 6.45 J (green line in Figure 5)) is required to trigger the perching mechanism. The minimum kinetic energy is higher than the required energy predicted by the model for potential energy in the linear springs (Table 1, linear energy (b) to (c)), indicating a loss of 1.2 J. This can be accounted for by losses in the system due to inefficiencies caused by sources such as friction and fluid drag. However, the minimum impact speed required for triggering the mechanism is smaller than the stall speed of the UAV ( $7 \text{ m s}^{-1}$ ).

In addition to the minimum triggering speed, it is important to understand how precisely the vehicle must approach the horizontal structure. To understand this, we first characterized the range of horizontal (yaw) angles at which the vehicle can impact the structure and successfully perch (Figure 6a). The same setup as the previous experiment was used; however, the height remained a constant 3.5 m and the relative yaw angle of the pole was adjusted. At  $14^\circ$  the perching was 100% successful, at  $29^\circ$  the success rate dropped to 20%, and at  $53^\circ$  the success rate was 0% (Figure 6a). As the perching system is symmetric, this indicates a range of successful perching between  $-29^\circ$  and  $29^\circ$ , or a span of  $58^\circ$ . The reason for this large span is that at high yaw angles the impact force gets projected perpendicular to the direction of travel (blue arrow in Figure 6a), which causes a moment about

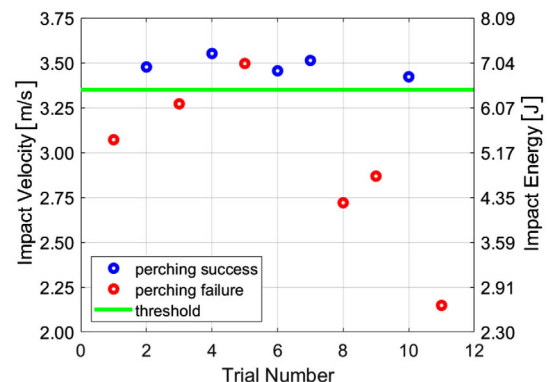
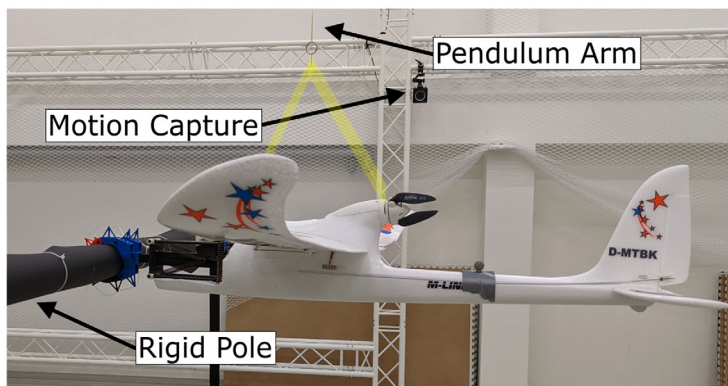


**Figure 5.** Left: Photograph of the pendulum setup. The plane swings from the upper right corner in an arc to the pole. Right: Plot of 11 trials at a variety of impact speeds and the corresponding impact energies. In blue are the successful perches and in red are the unsuccessful perches. The green line indicates an approximate threshold below which the vehicle is unable to perch. Yellow highlighting is used to show the cable holding the airplane.

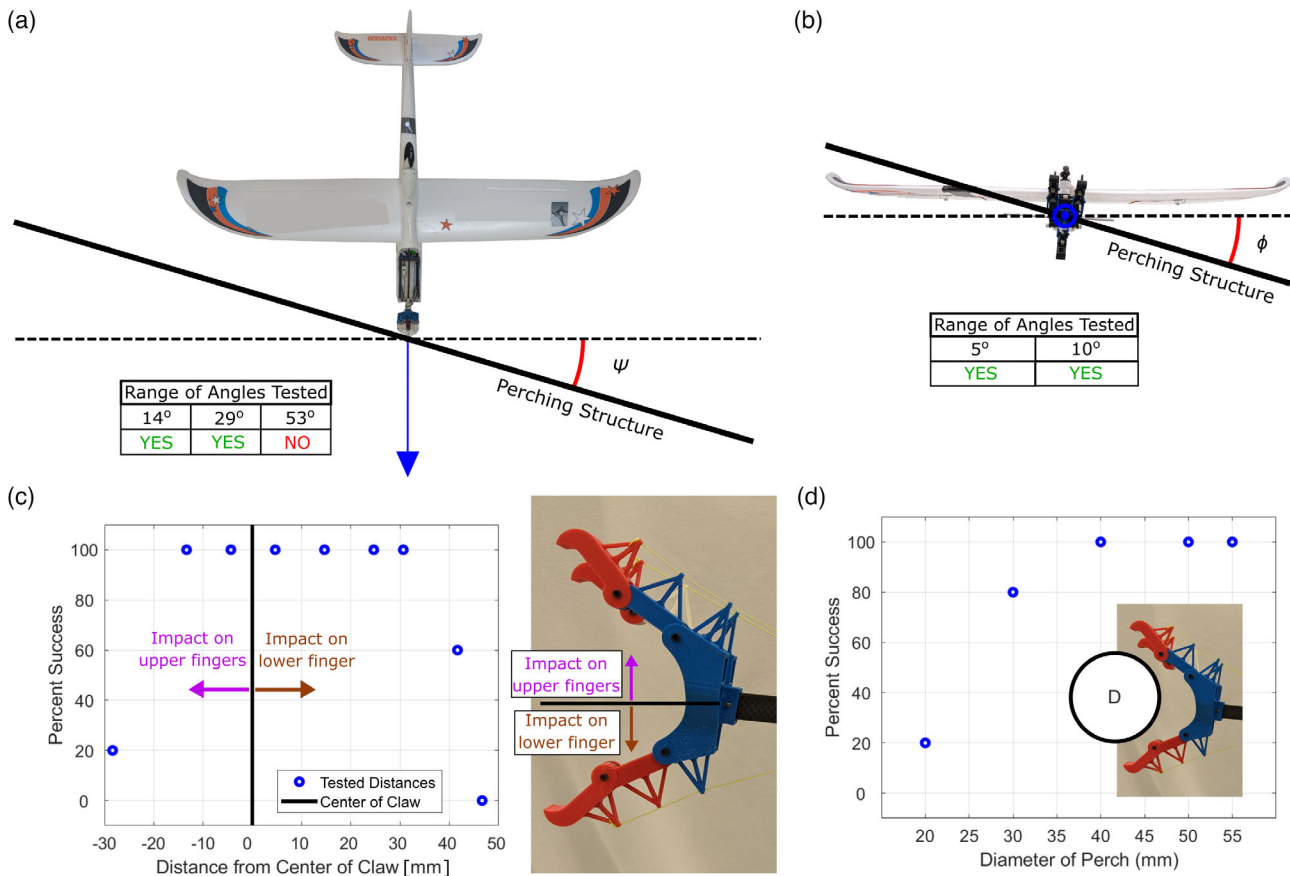


**Figure 6.** Overview of variations tested in the experiments. a) Illustration of the measured yaw impact angle. When tested at 14° and 29°, the aircraft was able to perch with 100% success rate. Above 29°, the UAV could not perch at all. b) Illustration of the measured roll impact angle. When tested at 5°, the aircraft was able to perch with 60% success and at 10° with 20% success rate. c) Results of characterization of vertical offset. Blue circles indicate the success rate of five trials at a given distance from the center of the claw. The vertical black line indicates the center of the claw. Left of the black line are impact points above the center of the claw and to the right of the black line are impact points below the center of the claw. d) Results of characterization of a variety of diameters. Blue circles indicate the success rate of five trials at a given diameter.

the center of gravity of the UAV. The resistance to rotation in this direction is low compared to pitch or roll and this allows the vehicle to self-adjust itself to be perpendicular to the structure. However, because a portion of the force is projected, the force component that compresses the linear springs is decreased. Ultimately, this limited the yaw angle at which the aircraft can perch. To verify this hypothesis, we took the data from the successful perpendicular runs and calculated the component of the force in the direction of travel.

$$E_{\text{yaw}} = E_{\text{perp}} \cos(\psi) \quad (4)$$

where  $E_{\text{perp}}$  is the energy from Figure 5 in J,  $\psi$  is the yaw angle in degrees, and  $E_{\text{yaw}}$  is the portion of the  $E_{\text{perp}}$  acting in the direction of flight. For  $\psi = 14^\circ$ , all the successful perches in Figure 5 maintain an energy level at or above the minimum required for successful perching (6.45 J). This indicates an expected 100% success rate, which matches the yaw angle variation experiment. Whereas for  $\psi = 53^\circ$ , none of the successful perches have

enough energy to successfully perch, matching the 0% success rate of the experiment.

To test the claw effectiveness at different roll angles, we simply adjusted the pole angle. Again, we released the aircraft from 3.5 m and used the same definition of success (once in five runs). Two angles were tested, 5° roll and 10° (Figure 6b). Both were successful; however, 5° was successful 60% of the time and 10° only 20%. This is a much smaller range of angles than with yaw (20° instead of 58°). When increasing the yaw angle, the component of the force that compresses the springs decreased, but with roll, that component does not change. However, the resistance of the UAV to rotation in the roll direction is much higher, as this rotation pushes the wing planform area against the air. As a result, the UAV was not able to perch beyond 10°. We also characterized the maximum vertical offset within the claw at the point of impact (Figure 6c). Once again, the same experimental setup described above was used. This time the length of the pendulum arm was adjusted with turnbuckles to raise and lower the aircraft relative to the horizontal perching structure. At each impact point, a total of five runs were done with a kinetic energy of

at least 6.45 J. The number of successful perching out of those five was recorded. A total of ten tests across a range of 8 cm were tested.

An asymmetry in the perching performance can be seen in the data (Figure 6c). The perching success rate is high when hitting the structure within a region between 15 mm above and 30 mm below the center of the claw. This asymmetry is likely due to the design of the claw, which has two fingers at the top of the claw and one finger at the bottom. When the bottom of the claw hits the structure, the lower stiffness of the single finger better shifts the airplane to center the structure in the claw, enabling it to successfully perch on the structure. The opposite is true when the impact point coincides with the top fingers of the claw.

Finally, we characterized how small of diameter a structure can be perched on (Figure 6d). The results indicate that below 40 mm there is a degradation in success. Failures at these diameters were due to slipping. The linear springs would lock in place, but the bar would slip out of the fingers. Success could be improved by changing the coefficient of friction with a coating on the finger tips or making the fingers out of a different material.

Once triggered, the claw must be able to hold the weight of the aircraft while it hangs there. We characterized this holding strength experimentally in an Instron 5965 machine (Figure 7). The sled of the claw was mounted to the lower clamp on the Instron and a 3D-printed stand-in for the pole with a 2 cm diameter was mounted to the top clamp. The Instron machine slowly pulled the stand-in upward at  $25 \text{ mm min}^{-1}$  and out of the fingers of the claw. The Instron machine was equipped with a 500 N loadcell which measured the force on the stand-in. The Instron machine simultaneously records how far the two clamps have moved. The experiment was repeated 4 times.

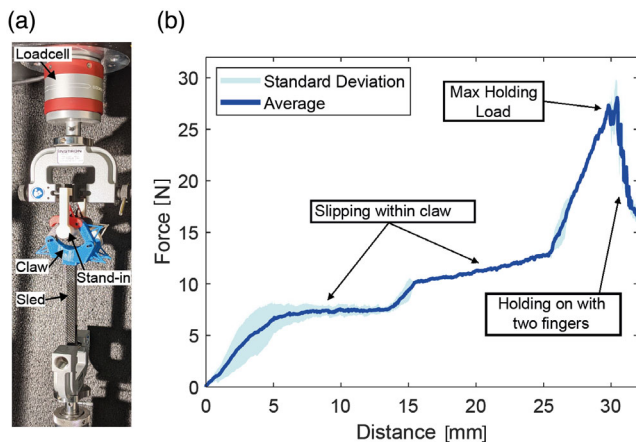


**Figure 7.** a) Photograph of the holding force characterization setup. The sled is anchored to the bottom of the machine, and the Instron machine pulls the loadcell upward, causing the stand-in to pull against the claw. This simulates the weight of the aircraft pulling against the claw. b) Data from the holding force characterization. In dark blue is the average of 4 runs and in light blue the standard deviation. The x-axis is the measured distance the Instron machine pulled the stand-in, and the y-axis is the simultaneously measured force. Slipping on the phalanges occurs between 5 and 13 mm and again between 15 and 25 mm. At 28 mm, the maximum sustained holding force is reached and one of the fingers slipped off the stand-in.

As the Instron pulled the pole stand-in out of the claw, the load increased steadily until the displacement reached about 5 mm (Figure 7b). At this point the stand-in slipped within the claw and the loading increased with a much shallower slope. These slips result from locations where the local friction force is less than the pulling force. The claw slips for a short distance before stopping. At about 13 mm the load began to increase again. This point indicates the end of the slip. A second slip within the claw occurred between about 16 and 25 mm. Finally, the loading reached a maximum of 28 N at about 30 mm. The loading dropped off at this point because one of the fingers slipped off the stand-in and the claw was left with just two fingers holding on. We took this condition as failure and ended the experiment. A maximum load of 28 N corresponds to the weight of a 2.9 kg aircraft, more than 3 times that of the aircraft used in these experiments (0.85 kg).

Finally, we validated the unperching strategy. To do this we attached the pole stand-in from the Instron tests to the end of the pendulum (Figure 8). We hung the aircraft by the claw from the pole stand-in and raised it to a height of just under 5 m above the ground. The ailerons and rudder were set to zero deflection, while the elevator was set to deflected fully upward. Motion capture markers were installed on the fuselage and one on each wing. Using a small servo, we triggered the claw release, causing the aircraft to fall. As the aircraft fell its instability caused the UAV to flip itself toward a nose-down orientation. After a drop of about 3 m, the UAV had rotated  $90^\circ$  such that it was belly-up (where the blue line crosses the black ones in Figure 8). It continued this rotation until it was almost vertical again, nose-down. At this point, the UAV impacted the ground. Data from the motion capture system indicated that at impact the UAV was pitched at  $8^\circ$  off of vertical.

Once the aircraft has fully rotated into the nose-down position, it needs to recover to level flight. This requires a  $90^\circ$  pitch-up turn, which will add more drop height to the experimentally measured flip. There is not enough height in the motion capture hall to experimentally measure the distance required for the pitch-up, so instead we estimate it. To calculate this drop distance, we follow the method given in the study by Anderson.<sup>[21]</sup> Lift, weight, and speed of the UAV are input into the model, which then outputs a turn radius. The pitch-up is a very dynamic maneuver for which standard static lift coefficients will not predict the lift accurately enough. Measuring or calculating dynamic lift coefficients is time-consuming and requires a complex test setup, so for this article, we use the dynamic lift coefficient of a similar aircraft, the Bixler 2, reported in the study by Greatwood et al.<sup>[22]</sup> Details of the derivation and calculations can be found in Note S2, Supporting Information.

Using that lift coefficient and data from the motion capture system,  $R$  can be estimated as 2.9 m. The motion capture data were also used to estimate the rotation rate of the aircraft just before impact, and that, in turn, was used to calculate that the vehicle needed another 0.1 m to reach a perfectly nose-down orientation. Combining the 5 m drop, with the extra 0.1 m needed for complete rotation and the 2.9 m turn radius gives an estimated 8 m to reorient to level flight. This analysis uses an approximation of the dynamic lift coefficient, specifically by taking the closest turn rate reported in the study by Greatwood et al.<sup>[22]</sup> It also assumes that once the turn has completed the vehicle is

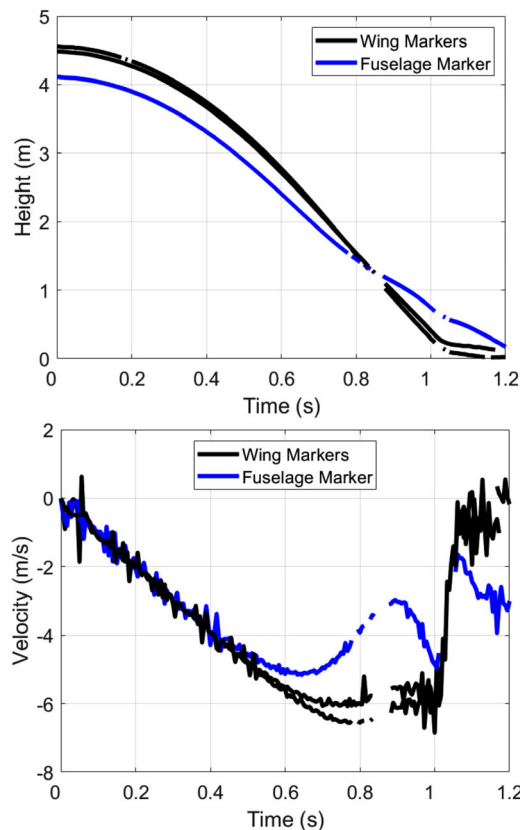


**Figure 8.** Results of the drop test. On the left are plots of the height and velocity of the aircraft as it falls. Gaps in the data are due to the motion capture cameras losing track of the markers.

traveling at least at stall speed, and would not continue to lose altitude. The experiment and analysis presented here is to give an idea of how much space is needed to reach horizontal flight after unperching. It was conducted using an off-the-shelf UAV, thus potentially better performance could be achieved with a purpose built vehicle that is more acrobatic. The total distance required to achieve horizontal flight could be further minimized through active control such as the use of the motor or control surfaces.

## 5. High-Speed Perching Tests

The pendulum setup in the previous experiments indicated that the minimum required speed to successfully trigger the claw and perch is  $3.35 \text{ m s}^{-1}$ . However, this setup cannot be used to reach minimum speed for the Easystar II ( $7 \text{ m s}^{-1}$ ). A separate setup is needed to validate the claws performance at higher speeds. To this end, a sling was used to reach the required flight speeds within the space of the motion capture hall (Figure 9). It consisted of a long elastic cable with one end anchored to one wall, and a loop on the other end which was hooked to the aircraft. The cable was stretched by pulling on the aircraft until it reached the far wall from the anchor point. Once released, the aircraft was pulled by the cable across the motion capture hall. A ramp built of extruded aluminum beams and PVC pipes guided the aircraft up and to the

perching structure. In addition to tracking the aircraft with the Optitrack motion capture system to measure its speed, high-speed footage of the perch was recorded at 1000 frames per second. The high-speed test can be viewed in the Supplementary Video.

The aircraft was slung into the structure successfully perching 3 times out of four attempts, impacting at an average of  $7.4 \text{ m s}^{-1}$ . High-speed camera footage indicates that the triggering mechanism successfully latched within 20 ms. The high speed of the impact caused the linear springs to bottom out at the end of the channel. At this point the force was transferred to the rigid structure of the fuselage. The foam fuselage was able to withstand the impact loads without problem; however, there was a recoil force once the springs bottomed out. Nevertheless, the rotational springs were able to hold the vehicle on the bar. Future studies could look at ways to improve the holding force of the claw through a coating on the claw to increase friction, or an active approach such as electroadhesion or geckoadhesion.

## 6. Discussion

In this article, we described a perching strategy for winged UAVs that absorbs and stores kinetic energy for unperching and experimentally characterized a prototype claw mechanism in indoor experiments. Our system does not require the dramatic speed reduction used in pitch-up perching maneuvers and is capable



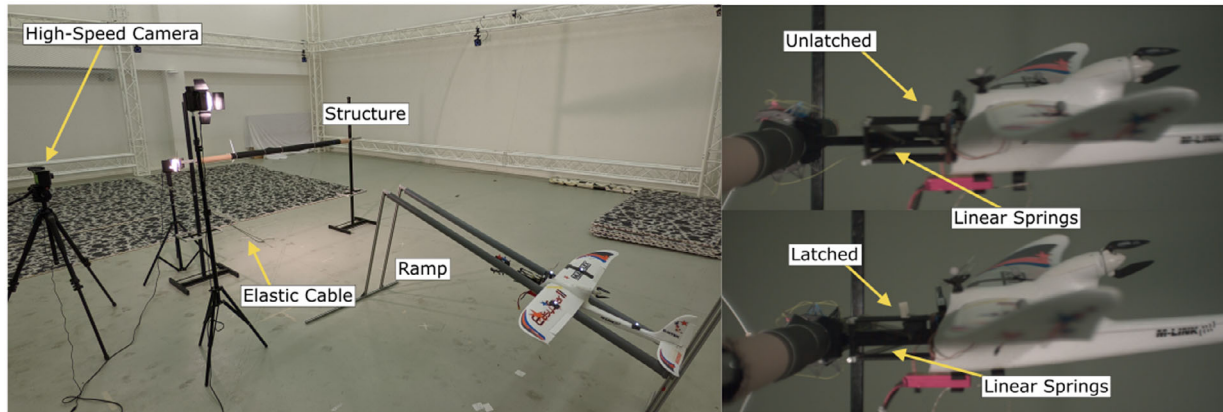


**Figure 9.** Left: A photograph of the ramp and sling test setup. Right: Still images from the high-speed camera showing the point of impact (top) and the latch in the closed position (bottom). These two still images from the 1000 fps video are separated by 20 frames.

of one of the fastest perching maneuvers to date at  $7.4 \text{ m s}^{-1}$ . We found that the claw is effective at a wide range of yaw impact angles ( $58^\circ$ ), but a smaller range in roll ( $20^\circ$ ). We attribute this to the vehicles resistance to rotation in these directions. In future systems based on this work, the range of angles could be improved by adding some compliance between the claw and the fuselage, allowing the claw itself to rotate rather than the entire aircraft. We also investigated the effect of a linear offset from the center of the claw at impact. We found that the impact point cannot vertically deviate more than 4.4 cm from the central shaft. Current top-of-the-line GPS technology in good conditions can provide cm accuracy, thus future implementation of a control system should be able to perch autonomously.<sup>[23]</sup> As these control systems mature, it will become ever easier to implement our perching strategy, and avoid the dangers of a pitch-up maneuver.

The claw on the front of our UAV is not particularly streamlined. This is because we left our mechanism exposed to better access different parts and better see its functioning. Higher technology readiness level (TRL) versions of it could incorporate a lightweight fairing, similar to the ones used by rockets. It could be attached to the outside of fingers allowing it to open and close with the claw. In addition to increased drag, the perching mechanism adds a bit of weight to the nose of the aircraft. This has the effect of shifting the CG forward, increasing the static margin, and in general makes the aircraft more stable. Having the CG too far forward means the vehicle must fly at a higher angle of attack, which increases drag. This can be mitigated through management of the CG by placing heavier items such as the battery and motor farther back.

Our energy capturing system was able to recapture 5% of the kinetic energy that would otherwise have been lost, but could be further improved by adopting more sophisticated mechanisms. For comparison, selfwinding watches usually recapture 46% of the motion energy<sup>[24]</sup> and regenerative braking on cars can get more than 25%.<sup>[25]</sup> Although we used the stored energy to unperch, there is no reason why this energy could not be used for other purposes such as powering active sensors (i.e., lidars and cameras), multimodal locomotion (i.e., crawling or rolling along the ground), or using actuators to interact with the

environment (i.e., performing a maintenance task on the perched infrastructure).

We have focused on applications for rigid infrastructure such as the trusses found on cranes and bridges. However, applications for perching on cables such as powerlines, railroad catenary, and cable-cars would benefit from perching UAVs as well. This will require further studies on how to balance the stiffness of the linear springs with the stiffness of the structure. If the cable has slack in it, instead of compressing the linear springs at impact, the cable could move.

To scale up the system, a few considerations would need to be addressed. The kinetic energy of the system is a function of mass and velocity, so increasing mass would require a decrease in velocity. This may put the successful trigger speed below the stall speed of the aircraft. Instead of reducing speed, stiffer springs could be used to absorb more of the kinetic energy of the impact. Finally, as mass increases, so would the potential for damage to the perching structure. Thus, much larger aircraft would need to consider more carefully what exactly they are perching on. Future systems, particularly for commercial applications, would also benefit from an impact analysis that could better predict the time of impact given the scale of the vehicle and impact speed. Due to the complexity of these models, and the fact that they require many material and design properties, this analysis was left out of this article.

Perching opens up opportunities for UAVs to spend an extended time sensing and relaying communication signals. In some cases it will be possible to recharge batteries, either through solar panels, or recharging by induction on powerlines. Our strategy is broadly applicable to the field of UAVs and with some optimization could be used to greatly increase their performance, and therefore applicability. The technology demonstrated in this article is in place for when perception and control technology has advanced to the point where it is possible to track long linear infrastructure to perch on.

## Supporting Information

Supporting Information is available from the Wiley Online Library or from the author.

## Acknowledgements

The authors gratefully acknowledge Olexandr Gudozhnik and Harry Vourtsis for their valuable contribution on the hardware and experimental setups. The authors also thank Enrico Ajanic for the useful discussions. This work was partially funded by the European Union's Horizon 2020 research and innovation program under grant agreement ID: 871479 AERIAL-CORE as well as the Swiss National Science Foundation through the Swiss National Centre of Competence in Research (NCCR) Robotics.

## Conflict of Interest

The authors declare no conflict of interest.

## Data Availability Statement

Research data are not shared.

## Keywords

aerial systems, energy recuperation, passive perching

Received: July 30, 2021

Revised: October 15, 2021

Published online:

- 
- [1] C. E. Doyle, J. J. Bird, T. A. Isom, J. C. Kallman, D. F. Bareiss, D. J. Dunlop, R. J. King, J. J. Abbott, M. A. Minor, *IEEE/ASME Trans. Mechatron.* **2013**, *18*, 506.
- [2] M. Tieu, D. M. Michael, J. B. Pflueger, M. S. Sethi, K. N. Shimazu, T. M. Anthony, C. L. Lee, in *Proc. SPIE 9797, Bioinspiration, Biomimetics, and Bioreplication*, Las Vegas, USA **2016**.
- [3] A. McLaren, Z. Fitzgerald, G. Gao, M. Liarokapis, in *2019 IEEE/RSJ Int. Conf. on Intelligent Robots and Systems (IROS)*, IEEE, Piscataway, NJ **2019**, pp. 5602–5607.
- [4] M. T. Pope, C. W. Kimes, H. Jiang, E. W. Hawkes, M. A. Estrada, C. F. Kerst, W. R. T. Roderick, A. K. Han, D. L. Christensen, M. R. Cutkosky, *IEEE Trans. Rob.* **2016**, *33*, 38.
- [5] E. W. Hawkes, D. L. Christensen, E. V. Eason, M. A. Estrada, M. Heverly, E. Hilgemann, H. Jiang, M. T. Pope, A. Parness, M. R. Cutkosky, in *2013 IEEE/RSJ Int. Conf. on Intelligent Robots and Systems*, IEEE, Piscataway, NJ **2013**, pp. 5487–5493.
- [6] H. Jiang, M. T. Pope, E. W. Hawkes, D. L. Christensen, M. A. Estrada, A. Parlier, R. Tran, M. R. Cutkosky, in *2014 IEEE Int. Conf. on Robotics and Automation (ICRA)*, IEEE, Piscataway, NJ **2014** 3102–3108.
- [7] M. A. Graule, P. Chirarattananon, S. B. Fuller, N. T. Jafferis, K. Y. Ma, M. Spenko, R. Kornbluh, R. J. Wood, *Science* **2016**, *352*, 978.
- [8] K. Hang, X. Lyu, H. Song, J. Stork, A. Dollar, D. Kragic, F. Zhang, *Sci. Robot.* **2019**, *4*, 28.
- [9] K. Zhang, P. Chermprayong, T. M. Alhinai, R. Siddall, M. Kovac, in *2017 IEEE/RSJ Int. Conf. on Intelligent Robots and Systems (IROS)*, IEEE, Piscataway, NJ **2017**, pp. 6849–6854.
- [10] H.-N. Nguyen, R. Siddall, B. Stephens, A. Navarro-Rubio, M. Kovac, in *2019 2nd IEEE Int. Conf. on Soft Robotics (RoboSoft)*, IEEE, Piscataway, NJ **2019**, pp. 80–87.
- [11] Y. H. Hsiao, P. Chirarattananon, *IEEE/ASME Trans. Mechatron.* **2019**, *24*, 2316.
- [12] R. Cory, R. Tedrake, in *AIAA Guidance, Navigation and Control Conf. and Exhibit*. American Institute of Aeronautics and Astronautics, Honolulu, HI **2008**.
- [13] E. Glassman, A. L. Desbiens, M. Tobenkin, M. Cutkosky, R. Tedrake, in *2012 IEEE Int. Conf. on Robotics and Automation*, IEEE, Piscataway, NJ **2012**, pp. 2235–2242.
- [14] A. Waldock, C. Greatwood, F. Salama, T. Richardson, *J. Intell. Rob. Syst.* **2018**, *92*, 685.
- [15] *Biomimetic and Biohybrid Systems*, (Ed: D. Mehanovic, J. Bass, T. Courteau, D. Rancourt, A. Lussier Desbiens, In M. Mangan, M. Cutkosky, A. Mura, P. F. Verschure, T. Prescott, N. Lepora), Lecture Notes in Computer Science, Springer International Publishing, Cham **2017**, pp. 302–314.
- [16] M. Anderson, in *47th AIAA Aerospace Sciences Meeting Including The New Horizons Forum and Aerospace Exposition*, Orlando, USA **2009**.
- [17] J. Anderson, *Fundamentals of Aerodynamics*, 4th ed., McGraw Hill, New York **2007**.
- [18] M. Kovac, J. M. Germann, C. Hürzeler, R. Siegwart, D. Floreano, *J. Micro-Nano Mechatron.* **2010**, *5*, 77.
- [19] T. Fahed, A. Gray, I. Hassan, S. Lofy, A. Mashfiqzaman, M. Melnyk, N. Skalamera, A. Todd, Ph.D. thesis, *Naval Postgraduate School*, **2018**.
- [20] In the Air With Zipline's Medical Delivery Drones - IEEE Spectrum, <https://spectrum.ieee.org/robotics/drones/in-the-air-with-ziplines-medical-delivery-drones> (accessed: July 2021).
- [21] J. D. Anderson, *Introduction to Flight*, 6th ed., McGraw-Hill Higher Education, McGraw-Hill **2008**.
- [22] C. Greatwood, A. Waldock, T. Richardson, *Aerosp. Sci. Technol.* **2017**, *71* 510.
- [23] RTK DP0601 GNSS (ZED-F9P) by Drotek, <https://store-drotek.com/891-rtk-zed-f9p-gnss.html> (accessed: July 2021).
- [24] L. Xie, C. G. Menet, H. Ching, R. Du, *J. Mech. Des.* **2009**, *131*, 7.
- [25] W. Liu, H. Qi, X. Liu, Y. Wang, *Front. Mech. Eng.* **2020**, *15*, 166.